PINK1-parkin-mediated mitophagy generates stereotyped somatic mosaicism of the mitochondrial genome

Arnaud Ahier, Chuan-Yang Dai, and Steven Zuryn*.

The University of Queensland, Queensland Brain Institute, Clem Jones Centre for Ageing Dementia Research, Brisbane, Australia.
**Corresponding author.*

Abstract

Mitochondria are critical for complex life and are characterized by the presence of their own genome (mtDNA). The mtDNA makeup within each cell is in a constant state of flux through processes of mutation, replication, and degradation, resulting in a mosaic mtDNA landscape that inevitably varies between cells, tissues, and organs within individuals. However, despite the stochastic nature of these processes, mosaic patterns of mtDNA mutations can become stereotyped across the tissues of individuals in both invertebrate and vertebrate species. The mechanisms that determine the non-random spatiotemporal distribution of mtDNA mutations are unknown. We find that PTEN induced putative kinase (PINK1) and the E3 ubiquitin-protein ligase parkin drive the formation of mtDNA heteroplasmy disparity between the major somatic tissue types of *C. elegans*, generating a stereotyped genetic mosaicism of the mitochondrial genomic landscape. PINK1 and parkin are conserved mediators of mitochondrial autophagy (mitophagy), but while PINK1/parkin preferentially direct the removal of mtDNA mutations in neurons, intestinal cells, and hypodermal cells, they act non-selectively in muscle cells to reduce mitochondrial network volume. These data suggest that different cell types use alternative strategies to cope with mtDNA mutations and implicate the nuclear genome encoded PINK1/parkin signalling axis in shaping stereotyped mitochondrial genomic mosaicism across individuals.

Introduction

Mitochondria act as central hubs for cellular bioenergetics, co-factor and macromolecule precursor synthesis, redox balance, Ca^{2+} handling, apoptosis, and immunity (Spinelli and Haigis, 2018; West and Shadel, 2017). These organelles house their own genome (mtDNA), as well as RNA and protein-synthesizing systems that together code and coordinate the

35 assembly of core subunits of the oxidative phosphorylation (OXPHOS) machinery used to
36 generate the cell's primary energy substrate, ATP. Although mtDNA lesions that perturb
37 OXPHOS assembly can cause devastating metabolic disorders (Gorman et al., 2016),
38 mutations are buffered by the polyploidy of the mitochondrial genome. Hundreds to
39 thousands of mtDNA copies can populate each cell, which can result in a mixture of multiple
40 mtDNA variants within individual cells and organelles (Morris et al., 2017). This state, termed
41 heteroplasmy, and the factors that influence its dynamics are critical determinants for the
42 pathogenesis of rare mitochondrial diseases, and possibly a wide range of common age-onset
43 inflictions, including neurodegeneration, diabetes, and cancer (Hahn and Zuryn, 2018;
44 Stewart and Chinnery, 2015).
45
46 At any given time, an interplay between stochastic and deterministic processes
47 influence cellular heteroplasmy (Hahn and Zuryn, 2018). Mitotic segregation, genetic drift,
48 and the competing effects of homeostatic (Gitschlag et al., 2016; Kandul et al., 2016; Lin et
49 al., 2016; Suen et al., 2010; Valenci et al., 2015) and retrograde signalling pathways (Gitschlag
50 et al., 2016; Lin et al., 2016) may contribute to the divergence of heteroplasmy levels between
51 the cells within a tissue, creating heteroplasmy mosaicism. However, there is evidence that
52 specific organs and tissues are prone to accumulating certain mtDNA mutations more than
53 others, leading to a stereotyped pattern of heteroplasmy mosaicism (Ahier et al., 2018;
54 Samuels et al., 2013; Soong et al., 1992; Wang et al., 2001). For example, the caudate,
55 putamen and substantia nigra regions of the brain show an age-dependent increase in the
56 heteroplasmy levels of the mtDNA^{4977} deletion (a mutant genome harbouring a 4,977bp
57 deletion), relative to the rest of the brain (Soong et al., 1992). In the invertebrate *C. elegans*,
58 stereotyped heteroplasmy differences have also been observed. Here, mtDNA molecules
59 harbouring a large deletion accumulate at different heteroplasmy levels in distinct somatic
60 and germ lineages in a reproducible manner (Ahier et al., 2018). However, it is unknown how
61 these non-random patterns mtDNA heteroplasmy between tissues evolves within individuals.
62
63 Here, we have determined that cell-type-specific roles for PTEN-induced putative
64 kinase 1 (PINK1) and the E3 ubiquitin-protein ligase parkin generate stereotyped patterns of
65 mtDNA mosaicism across major somatic tissues in *C. elegans*. PINK1 and parkin are conserved
66 mediators of mitochondrial autophagy (mitophagy), a selective form of autophagy that

67 removes depolarized mitochondria (Palikaras et al., 2018). The defective organelles are
68 decorated with polyubiquitin chains on their outer surface via PINK1 recruitment of parkin,
69 and are subsequently captured by autophagosomes and destroyed following fusion with
70 lysosomes (Harper et al., 2018). We show that mutations in PINK1 and parkin reverse the
71 stereotyped divergence of mtDNA heteroplasmy observed between neuronal, muscle,
72 intestinal, and hypodermal tissue types. Moreover, we reveal that distinct tissue types use
73 unique strategies to manage mtDNA mutations, which may be dependent upon metabolic
74 requirements. Our results provide a mechanistic rationale for stereotyped mtDNA mosaicism
75 in the soma and provide insights into the processes that contribute to the evolving mtDNA
76 landscape within individuals in both healthy and diseased states.
77
78 **Results and Discussion**
79 In order to determine whether conserved homeostatic mechanisms such as mitophagy shape
80 stereotyped mosaic patterns of somatic mtDNA distribution, we introduced a heteroplasmic
81 variant of mtDNA that harbours a 3.1 kb deletion (*uaDf5*, also called ΔmtDNA) (Tsang and
82 Lemire, 2002) into double-mutant strains with null deletions in the genes PINK1 (*pink-1*) and
83 parkin (*pdr-1*). The *uaDf5* deletion exists in heteroplasmy with wild-type copies of the mtDNA
84 at a level of approximately 60% across populations of animals (Lin et al., 2016; Tsang and
85 Lemire, 2002). We next crossed these triple mutant strains to transgenic animals carrying a
86 *mos1*-mediated single-copy insertion (mosSCI) of *TOMM-20::mKate2::HA* controlled by either
87 a pan-neuronal promoter (*rgef-1p*), intestinal-specific promoter (*ges-1p*), hypodermis
88 (epidermis)-specific promoter (*dpy-7p*), or body wall muscle (BWM)-specific promoter (*myo-*
89 *3p*). Using this panel of strains, we performed cell-type-specific mitochondrial affinity
90 purification (CS-MAP) (Ahier et al., 2018), allowing comparisons of mtDNA heteroplasmy
91 across major tissue types in animals lacking PINK-1-PDR-1-mediated mitophagy (Figure 1A).
92
93 Heteroplasmy in cell-type-specific mitochondria was investigated across very large
94 populations of pooled animals (>10,000 individuals, see methods). This approach enabled
95 population-scale trends to be resolved by overcoming confounding influences that can be
96 introduced by the presence of stochastic inter-individual variations in mosaicism.
97 Mitochondria were purified from both *pink-1(tm1779)*;*pdr-1(gk448)* double-mutant and wild-
98 type backgrounds carrying ΔmtDNA. To accurately quantify ΔmtDNA heteroplasmy levels

99 from each tissue type, we used a fluorescence multiplex quantitative PCR (qPCR) assay (Ahier
100 et al., 2018). To eliminate the influence of any inter-population variability affecting our
101 analyses, we compared mitochondria purified from each cell type to the total mitochondria
102 (homogenate) from the same samples. In addition, we performed the same experiments in
103 animals in which mitochondria from all cell types were purified using the same CS-MAP
104 technique. In this case, the ubiquitous promoter *etf-3p* was used to drive the expression of a
105 *TOMM-20::mKate2::HA* transgene integrated into the same genomic location as the other
106 transgenes. As expected, ΔmtDNA heteroplasmy levels did not change between total input
107 mitochondria and mitochondria purified from all cells of wild-type and *pink-1(tm1779)*;*pdr-*
108 *1(gk448)* backgrounds (Figure 1B). This confirmed that deficiencies in PINK-1 and PDR-1 did
109 not influence the CS-MAP procedure.
110
111 However, we found that removal of the PINK-1-PDR-1 mitophagy pathway in mitochondria
112 purified from neurons, intestine, and hypodermis resulted in a significant increase in ΔmtDNA
113 heteroplasmy levels (Figure 1B). This suggests that mitophagy operates within these tissues
114 to selectively remove ΔmtDNA molecules. In wild-type animals, mitochondria isolated from
115 neurons and intestinal cells displayed lower levels of heteroplasmy relative to the
116 homogenate. However, inactivating PINK-1-PDR-1-mediated mitophagy completely reversed
117 this trend, suggesting that PINK-1-PDR-1-dependent mitophagy is particularly important in
118 these cell types for maintaining heteroplasmy levels below the average for the whole animal
119 (Figure 1B). Interestingly, we found that removal of *pink-1* and *pdr-1* had no effect on ΔmtDNA
120 heteroplasmy levels in BWM cells, indicating that PINK-1-PDR-1-mediated mitophagy was not
121 utilised in this tissue type for mitochondrial genome quality control (Figure 1B and 1C).
122 Moreover, removal of *pink-1* and *pdr-1* abolished any differences in ΔmtDNA heteroplasmy
123 levels between all of the major tissue types studied (Figure 1D), suggesting that PINK-1-PDR-
124 1-mediated mitophagy acts to drive stereotyped mosaicism of the mitochondrial genome.
125
126 Different cell types have distinct functions and therefore have varying energetic demands.
127 The BWM is composed of four quadrants of somatic muscle bundles, each of which consists
128 of 23-24 cells arranged into staggered pairs that stretch longitudinally from the head to the
129 tail of the animal (Gieseler et al., 2017). The coordinated contractile activities of these bundles
130 produce powerful and energetically demanding sinusoidal body bends that drive locomotion.

131 We therefore hypothesised that BWM cells might avoid mitophagy in combating mtDNA
132 mutations so as to prevent reductions of the mitochondrial network. To test this idea, we
133 analysed the volume of mitochondria in all tissues using three-dimensional reconstruction of
134 fluorescence images acquired from strains carrying *TOMM-20::mKate2::HA* (Figure 2). We
135 found that the presence of ΔmtDNA tended to increase the volume of the mitochondrial
136 network in neurons, intestine, and hypodermis, although significant increases were only
137 observed in hypodermal tissue (Figure 2A-C and 2E-G). Mitochondrial volume remained
138 unchanged in BWM tissue in the presence of ΔmtDNA (Figure 2D and H). However, we found
139 that removal of *pink-1* and *pdr-1* in this background almost tripled the volume of the
140 mitochondrial network in BWM cells (Figure 2Dc and H). This suggests, as previously
141 demonstrated during ageing (Palikaras et al., 2015), that PINK-1-PDR-1-mediated mitophagy
142 controls the mitochondrial density in *C. elegans* BWM cells. However, unlike in other major
143 tissue types, mitophagy does not counteract the presence of deleterious mitochondrial
144 genomes in the muscle. In contrast, whereas PINK-1-PDR-1-mediated mitophagy appeared to
145 preferentially coordinate the removal of ΔmtDNA in the nervous system, intestine, and
146 hypodermis, it did not appear to play a role in shaping mitochondrial volume, which remained
147 unchanged when both *pink-1* and *pdr-1* were removed in ΔmtDNA backgrounds (Figure 2A-C
148 and 2E-G). One possible explanation for this observation is that cells with high energy
149 demand, such as muscle cells, stimulate high amounts of mitochondrial biogenesis that is
150 balanced through mitophagy-mediated removal. As such, under high mitochondrial turnover
151 conditions, mitophagy may fulfil a different primary role and therefore lose selectivity
152 towards the removal of genetically faulty mitochondria. Indeed, we found that mitophagy
153 restricted the mitochondrial networks to almost one third the volume they would otherwise
154 be in BWM cells, a workload that may saturate the mitophagy machinery. A similar role was
155 not observed in the other major tissue types. Moreover, in wild-type backgrounds, BWM cells
156 had the highest ΔmtDNA heteroplasmy levels of any somatic tissue type (Figure 1B),
157 suggesting that mtDNA quality control is, overall, less efficient in muscle.
158
159 The *uaDf5* deletion disrupts four genes that encode core subunits of the electron transport
160 chain and as such, ΔmtDNA is insufficient for the assembly of a functional OXPHOS system.
161 Despite this, we found that BWM activity was unperturbed by the presence of ΔmtDNA.
162 Animals carrying ΔmtDNA could still produce sinusoidal body bends under strenuous

163 conditions (thrashing assay, see materials and methods) at rates comparable to those of their
164 wild-type counterparts, even when genetically bottlenecked to very high heteroplasmy levels
165 (93.39 ± 0.34%) and tested at various ages up to 5-day old adults (Figure 3A). This suggested
166 that BWM cells could effectively compensate for the presence of deleterious mtDNA in order
167 to maintain function over their lifetimes. Recently demonstrated in mouse sperm, one
168 potential mechanism to compensate for deleterious heteroplasmic mtDNA mutations is to
169 increase the copy number of total mitochondrial genomes (Jiang et al., 2017). Although not
170 helping to remove or repair the mutations themselves, energy supplies might be restored if
171 the expression level of mtDNA-encoded components is increased through an indiscriminate
172 elevation in both mutant and wild-type genome copy number. We therefore investigated
173 whether BWM cells responded to the presence of ΔmtDNA by enhancing mtDNA replication.
174 Indeed, we found that in all tissues except hypodermis, the mtDNA copy number per
175 mitochondrion increased in the presence of ΔmtDNA (Figure 3B). However, the largest
176 absolute increase was observed in BWM mitochondria, with almost 2 additional copies of
177 mtDNA in each mitochondrion (Figure 3C). This suggests that BWM mitochondria have a
178 greater capacity to respond to ΔmtDNA by perpetuating a higher overall copy number of
179 mtDNA per mitochondrion, which may act as an alternative mechanism for maintaining cell
180 function in the absence of mitophagy-mediated mtDNA quality control.
181
182 Together, our results suggest that major and distinct tissue systems comprising the three
183 primary germ layers manage deleterious mtDNA mutations by differentially adopting
184 mitophagy and mtDNA biogenesis processes (Figure 3D). Moreover, we have determined that
185 stereotyped distribution patterns of mitochondrial genomes harbouring deletions are caused
186 by disparate roles of PINK-1-PDR-1-mediated mitophagy in different cell types. Interestingly,
187 large mtDNA deletions have been shown to follow stereotyped patterns of accumulation in
188 specific regions of the human brain during ageing (Soong et al., 1992). In the context of our
189 findings, it would be interesting to determine whether such changes are the result of
190 alterations in mitophagy processes in these cells. Indeed, the increase in heteroplasmy levels
191 observed following removal of *pink-1* and *pdr-1* was the greatest in the nervous system. This
192 suggests that neurons are heavily reliant upon mitophagy for the surveillance and removal of
193 mtDNA deletions. Accumulating evidence suggests that mtDNA mutations contribute to the
194 progressive nature of age-related neurodegenerative diseases (Stewart and Chinnery, 2015)

195 and mitophagy itself has also been shown to be disrupted in models of neurodegeneration
196 (Cummins et al., 2018; Ye et al., 2015). Indeed, mutations in both PINK1 (Valente et al., 2004)
197 and parkin (Kitada et al., 1998) cause early-onset Parkinson's disease, suggesting that
198 perturbations to mitophagy promote neurodegeneration, which in light of our results, may
199 be attributable to the nervous system's reliance on mitophagy for quality control of the
200 neuronal mtDNA landscape.
201
202 **Figures**

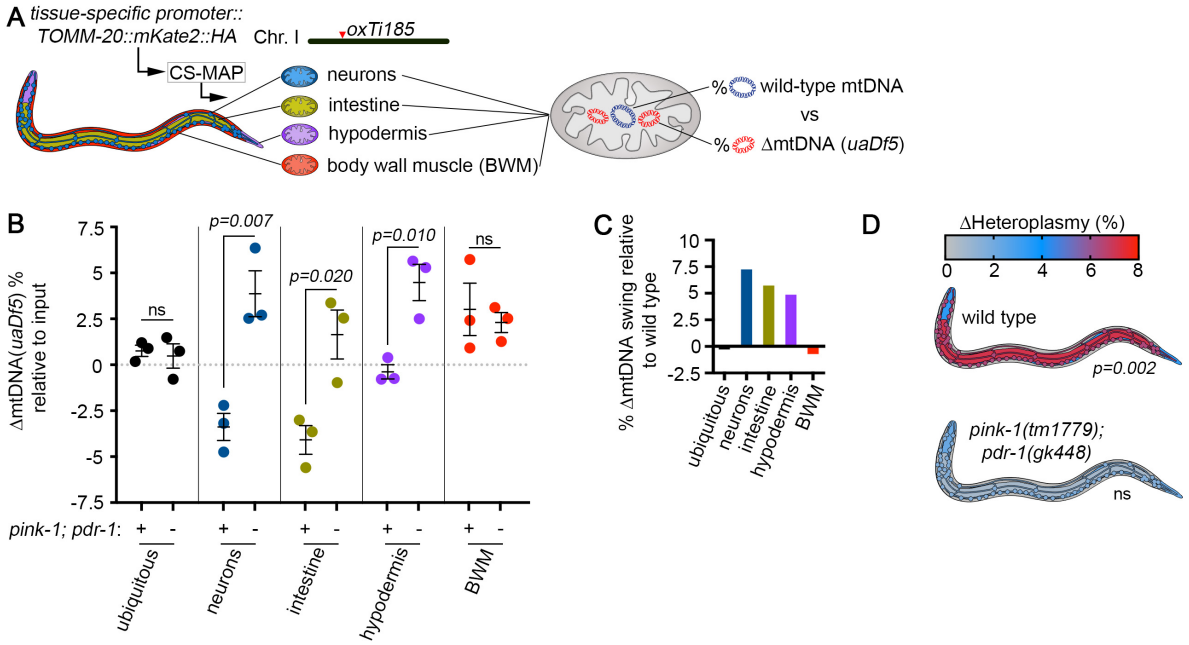

203
204 **Fig.1 *pink-1* and *pdr-1* determine stereotyped patterns of ΔmtDNA somatic mosaicism.** (**A**)
205 Schematic of *C. elegans* and mitochondria originating from major somatic tissue types.
206 *TOMM-20::mKate2::HA* transgenes driven by tissue-specific promoters were integrated into
207 the *oxTi185* site on chromosome 1. In these transgenic animals, cell-specific mitochondrial
208 affinity purification (CS-MAP) was used to purify mitochondria of each cell type from whole
209 animals. Mitochondria harbour both wild-type and ΔmtDNA (*uaDf5*) genomes, a situation
210 known as heteroplasmy. The percentages of each genome were quantified from each sub-
211 population of mitochondria obtained from each cell type. (**B**) Percentage of ΔmtDNA in
212 mitochondria purified from each tissue type, relative to total homogenate. +, animals with
213 functional *pink-1* and *pdr-1* genes; -, animals with deletions in *pink-1* and *pdr-1*. Bars are
214 means ± s.e.m. *P* values were determined using one-way ANOVA and Tukey's correction. (**C**)
215 Summary of the swing in ΔmtDNA % caused by deletion of *pink-1* and *pdr-1* genes, relative to

wild-type animals. (**D**) Graphical representation of the loss of stereotyped inter-tissue variation in ΔmtDNA heteroplasmy in *pink-1;pdr-1* double mutant animals. Each tissue type is coloured according to ΔHeteroplasmy, which is the difference in *uaDf5* heteroplasmy relative to BWM. The significance of heteroplasmy variation between tissues was calculated using one-way ANOVA.

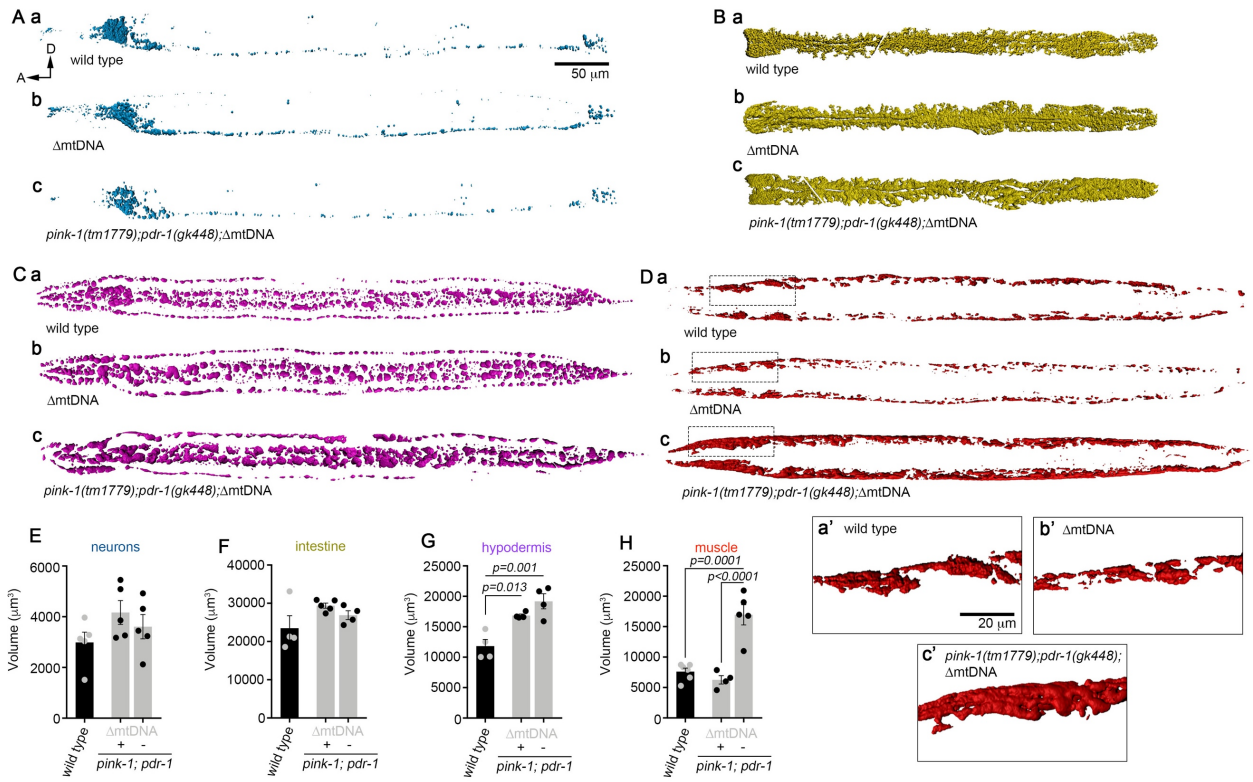

Fig. 2 PINK-1-PDR-1 mediated mitophagy controls mitochondrial network volume in muscle cells. (**A-D**) Representative three-dimensional reconstructions of *C. elegans* (**A**) Complete nervous system mitochondria, (**B**) intestinal mitochondria, (**C**) hypodermal mitochondria, and (**D**) body wall muscle (BWM) mitochondria in (**a**) wild-type animals, (**b**) animals harbouring ΔmtDNA, and (**c**) animals carrying ΔmtDNA in the absence of *pink-1* and *pdr-1* genes (**A-D**, scale bar, 50 μm). For (**D**), dashed boxes are magnified in (**a'-c'**) (scale bar, 20 μm). (**E-H**) Quantification of mitochondrial volumes from each tissue type. Columns are means ± s.e.m. of individual animals (dots). *P* values were determined using one-way ANOVA and Tukey's correction.

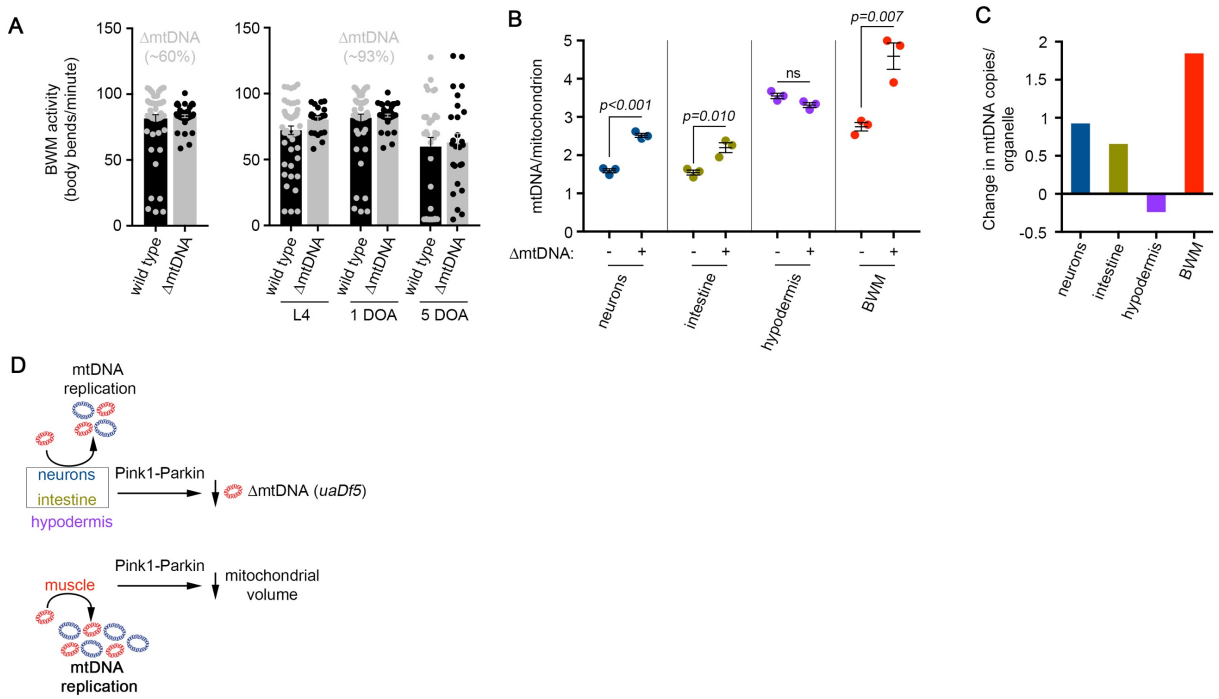

Fig. 3 Tissue-specific mtDNA replication in response to the presence of ΔmtDNA. (**A**) Quantification of body wall muscle (BWM) function using the thrashing assay. ΔmtDNA heteroplasmy levels are shown above each graph. Columns are means ± s.e.m. of individual animals (dots). Two-sided *t*-test. L4, larval stage 4; 1 DOA, 1-day old adult; 5 DOA, 5-day old adult. (**B**) Quantification of mtDNA molecules per mitochondrion (see materials and methods). -, animals not carrying ΔmtDNA; +, animals carrying ΔmtDNA. Bars are means ± s.e.m. *P* values were determined using one-way ANOVA and Tukey's correction. (**C**) Summary of change in mtDNA copy number per mitochondrion caused by the presence of ΔmtDNA, relative to wild-type animals. (**D**) Model summarizing the distinct mechanisms by which different cell types manage mtDNA deletions. Neurons, intestinal cells, and hypodermal cells use PINK-1-Parkin to reduce ΔmtDNA heteroplasmy levels, whereas muscle cells do not. Only neurons, intestinal cells, and muscle cells induce mtDNA replication in response to the presence of ΔmtDNA, with muscle cell mitochondria showing the greatest induction of this response.

Materials and Methods

***C. elegans* strains and culture**. LB138 *him-8(e1489) IV; uaDf5/+*; EG8078 *oxTi185 I; unc-119(ed3) III;* BR4006 *pink-1(tm1779) II; byEx655 [pink-1p::pink-1::GFP; myo-2p::mCherry; herring sperm DNA]*; VC1024 *pdr-1(gk448) III* and wild-type (N2) were acquired from the

252 *Caenorhabditis* Genetics Center (CGC), University of Minnesota, USA, which is funded by the
253 NIH Office of Research Infrastructure Programs (P40 OD010440). *C. elegans* culture and
254 maintenance were performed according to standard protocols (Brenner, 1974). The
255 transgenic strains used for cell-specific mitochondrial purification experiments were
256 generated as previously described (Ahier et al., 2018).
257
258 **Cell-specific Mitochondrial Affinity Purification (CS-MAP).** CS-MAP was performed as
259 previously described (Ahier et al., 2018). Briefly, 10,000 to 20,000 L4 staged worms were
260 grown on 2 x 150 mm NGM plates seeded with *E. coli* OP50 bacteria. Worms were
261 homogenised into a hypotonic buffer [50 mM KCl, 110 mM mannitol, 70 mM sucrose, 0.1 mM
262 EDTA (pH 8.0), 5 mM Tris-HCl (pH 7.4)] with a dounce homogenizer and the subsequent crude
263 mitochondrial fraction was enriched by differential centrifugations and mitochondria were
264 isolated from this fraction using anti-HA (Influenza Hemagglutinin) magnetic beads (Pierce).
265 Beads were washed and resuspended in 20 µl of hypotonic buffer. All CS-MAP experiments
266 were repeated in at least three independent experiments and data for each genetic
267 background were obtained at similar times as previously reported in Ahier et al., 2018 for
268 control wild-type backgrounds.
269
270 **mtDNA extraction and Quantitative PCR**. For all mtDNA analyses, total input and affinity-
271 purified mitochondria were lysed and extracted using phenol-chloroform-isoamyl alcohol,
272 followed by an ethanol precipitation. Extracted DNA was resuspended in 10 mM Tris-HCl (pH
273 8), 0.1 mM EDTA. Then, multiplex quantitative PCR was performed using the Luna Universal
274 Probe qPCR Master Mix (ref M3004, NEB), a Rotor Gene Q Real-Time PCR (Qiagen) Machine
275 and Rotor Gene Q pure detection software (V2.3.1). The primers 5'-
276 cgtaagaaaatcaaaatatggtataattgg-3', 5'-aaaatgttacgatccttattaataaagc-3', 5'-
277 gcagagatgtttattgaagctgac-3' and the probes 5'-HEX/tgaggccag/ZEN/ttcatattgttccaga
278 gtg/IABKFQ-3' (Iowa Black FQ) and 5'-6-FAM/ccatccgtg/ZEN/ctagaagacaaagaatttc/IABKFQ-3'
279 were used to quantify the wild-type mtDNA and ΔmtDNA levels. Calculations of mtDNA copies
280 per mitochondrion were derived from the quantification of purified organelles in individual
281 samples, as previously performed (Ahier et al., 2018). Control wild-type values are reported
282 in Ahier et al., 2018.
283

284 **Image acquisition and processing**. Imaging was performed on live animals mounted on a 2%
285 agarose pad on glass slides with 1 mM levamisole (Sigma). For quantification of purified
286 mitochondria, we visualized fluorescence using a Zeiss Z2 imager microscope with a Zeiss
287 Axiocam 506 mono camera and Zen2 (version 2.0.0.0) software. Mitochondria were counted
288 with the aid of the Image J Grid plugin, and comparisons were made on the same
289 immunoprecipitation volume for each sample. For 3D reconstruction, images were acquired
290 using a spinning-disk confocal system (Marianas; 3I, Inc.) consisting of an Aanio Observer Z1
291 (Carl Zeiss) equipped with a CSU-W1 spinning-disk head (Yokogawa Corporation of America),
292 ORCA-Flash4.0 v2 sCMOS camera (Hamamatsu Photonics), 20x 0.8 NA PlanApo and 40x 1.2
293 NA C-Apo objectives. Image acquisition was performed using SlideBook 6.0 (3I, Inc). 3D
294 reconstruction and mitochondrial volume calculations were performed using 3D rendering in
295 Imaris software (version 8.4.1, Bitplane). Imaging was performed at the Queensland Brain
296 Institute's Advanced Microscopy Facility.
297
298 **Thrashing assays**. Thrashing assays were performed on worms suspended in 40 µl of M9
299 buffer on a hydrophobic slide (ref G350308BK, ProSciTech). After an initial 3 min period, a 30
300 second video sequence of the thrashing animals was recorded using a Nikon SMZ745T
301 stereomicroscope and a TrueChrome IIS camera (Tucsen Photonics). Body bends per minutes
302 were determined using CeleST Computer Vision Software as described previously (Restif et
303 al., 2014).
304
305 **Statistics and Reproducibility**. Statistical analyses performed are described for each figure.
306 One-way analysis of variance (ANOVA) was performed for comparisons across multiple
307 independent samples, using Tukey's multiple comparisons correction. All experiments were
308 reproduced at least 3 times with similar results.
309
310 **Data and reagent availability.** All data and biological reagents that support the conclusions
311 of this manuscript are available from the corresponding author on request.
312
313 **Acknowledgements**
314 We are grateful to R. Tweedale for comments on the manuscript and members of the Zuryn
315 laboratory for discussions and comments. We also thank A. Gaudin for support with

316 microscopy. Some strains were provided by the CGC, which is funded by the NIH Office of
317 Research Infrastructure Programs (P40 OD010440). This work was supported by NHMRC
318 Project Grants GNT1128381 and GNT1162553, a Stafford Fox Senior Research Fellowship to
319 S.Z., and a University of Queensland International Scholarship to C.Y.D.
320

321 **Contributions**

322 A.A. carried out most experiments. C.Y.D., S.Z. contributed some experiments. A.A., C.Y.D and
323 S.Z. designed and interpreted experiments and wrote the paper.
324

325 **Competing Interest**

326 The authors declare that they do not have any financial or non-financial competing interests.
327

328 **References**

329 Ahier, A., Dai, C.-Y., Tweedie, A., Bezawork-Geleta, A., Kirmes, I., and Zuryn, S. (2018).
330 Affinity purification of cell-specific mitochondria from whole animals resolves patterns of
331 genetic mosaicism. Nat Cell Biol *20*, 352-360.

332 Brenner, S. (1974). The genetics of Caenorhabditis elegans. Genetics *77*, 71-94.

333 Cummins, N., Tweedie, A., Zuryn, S., Bertran-Gonzalez, J., and Gotz, J. (2018). Disease-
334 associated tau impairs mitophagy by inhibiting Parkin translocation to mitochondria. EMBO
335 J.

336 Gieseler, K., Qadota, H., and Benian, G.M. (2017). Development, structure, and maintenance
337 of C. elegans body wall muscle. WormBook *2017*, 1-59.

338 Gitschlag, B.L., Kirby, C.S., Samuels, D.C., Gangula, R.D., Mallal, S.A., and Patel, M.R. (2016).
339 Homeostatic Responses Regulate Selfish Mitochondrial Genome Dynamics in C. elegans. Cell
340 Metab *24*, 91-103.

341 Gorman, G.S., Chinnery, P.F., DiMauro, S., Hirano, M., Koga, Y., McFarland, R., Suomalainen,
342 A., Thorburn, D.R., Zeviani, M., and Turnbull, D.M. (2016). Mitochondrial diseases. Nat Rev
343 Dis Primers *2*, 16080.

344 Hahn, A., and Zuryn, S. (2018). The Cellular Mitochondrial Genome Landscape in Disease.
345 Trends Cell Biol.

346 Harper, J.W., Ordureau, A., and Heo, J.M. (2018). Building and decoding ubiquitin chains for
347 mitophagy. Nat Rev Mol Cell Biol *19*, 93-108.

348 Jiang, M., Kauppila, T.E.S., Motori, E., Li, X., Atanassov, I., Folz-Donahue, K., Bonekamp, N.A.,
349 Albarran-Gutierrez, S., Stewart, J.B., and Larsson, N.G. (2017). Increased Total mtDNA Copy

350 Number Cures Male Infertility Despite Unaltered mtDNA Mutation Load. Cell Metab *26*, 429-
351 436 e424.

352 Kandul, N.P., Zhang, T., Hay, B.A., and Guo, M. (2016). Selective removal of deletion-bearing
353 mitochondrial DNA in heteroplasmic Drosophila. Nat Commun *7*, 13100.

354 Kitada, T., Asakawa, S., Hattori, N., Matsumine, H., Yamamura, Y., Minoshima, S., Yokochi,
355 M., Mizuno, Y., and Shimizu, N. (1998). Mutations in the parkin gene cause autosomal
356 recessive juvenile parkinsonism. Nature *392*, 605-608.

357 Lin, Y.F., Schulz, A.M., Pellegrino, M.W., Lu, Y., Shaham, S., and Haynes, C.M. (2016).
358 Maintenance and propagation of a deleterious mitochondrial genome by the mitochondrial
359 unfolded protein response. Nature *533*, 416-419.

360 Morris, J., Na, Y.J., Zhu, H., Lee, J.H., Giang, H., Ulyanova, A.V., Baltuch, G.H., Brem, S., Chen,
361 H.I., Kung, D.K.*, et al.* (2017). Pervasive within-Mitochondrion Single-Nucleotide Variant
362 Heteroplasmy as Revealed by Single-Mitochondrion Sequencing. Cell Reports *21*, 2706-
363 2713.

364 Palikaras, K., Lionaki, E., and Tavernarakis, N. (2015). Coordination of mitophagy and
365 mitochondrial biogenesis during ageing in C. elegans. Nature *521*, 525-528.

366 Palikaras, K., Lionaki, E., and Tavernarakis, N. (2018). Mechanisms of mitophagy in cellular
367 homeostasis, physiology and pathology. Nature Cell Biology *20*, 1013-1022.

368 Restif, C., Ibanez-Ventoso, C., Vora, M.M., Guo, S.Z., Metaxas, D., and Driscoll, M. (2014).
369 CeleST: Computer vision software for quantitative analysis of C. elegans swim behavior
370 reveals novel features of locomotion. Plos Comp Biol *10*.

371 Samuels, D.C., Li, C., Li, B., Song, Z., Torstenson, E., Boyd Clay, H., Rokas, A., Thornton-Wells,
372 T.A., Moore, J.H., Hughes, T.M.*, et al.* (2013). Recurrent tissue-specific mtDNA mutations are
373 common in humans. PLoS Genet *9*, e1003929.

374 Soong, N.W., Hinton, D.R., Cortopassi, G., and Arnheim, N. (1992). Mosaicism for a Specific
375 Somatic Mitochondrial-DNA Mutation in Adult Human Brain. Nature Genetics *2*, 318-323.

376 Spinelli, J.B., and Haigis, M.C. (2018). The multifaceted contributions of mitochondria to
377 cellular metabolism. Nat Cell Biol *20*, 745-754.

378 Stewart, J.B., and Chinnery, P.F. (2015). The dynamics of mitochondrial DNA heteroplasmy:
379 implications for human health and disease. Nat Rev Genet *16*, 530-542.

380 Suen, D.F., Narendra, D.P., Tanaka, A., Manfredi, G., and Youle, R.J. (2010). Parkin
381 overexpression selects against a deleterious mtDNA mutation in heteroplasmic cybrid cells.
382 Proc Natl Acad Sci U S A *107*, 11835-11840.

383 Tsang, W.Y., and Lemire, B.D. (2002). Stable heteroplasmy but differential inheritance of a
384 large mitochondrial DNA deletion in nematodes. Biochem Cell Biol *80*, 645-654.

385 Valenci, I., Yonai, L., Bar-Yaacov, D., Mishmar, D., and Ben-Zvi, A. (2015). Parkin modulates
386 heteroplasmy of truncated mtDNA in Caenorhabditis elegans. Mitochondrion *20*, 64-70.

387 Valente, E.M., Abou-Sleiman, P.M., Caputo, V., Muqit, M.M., Harvey, K., Gispert, S., Ali, Z.,
388 Del Turco, D., Bentivoglio, A.R., Healy, D.G.*, et al.* (2004). Hereditary early-onset Parkinson's
389 disease caused by mutations in PINK1. Science *304*, 1158-1160.

390 Wang, Y., Michikawa, Y., Mallidis, C., Bai, Y., Woodhouse, L., Yarasheski, K.E., Miller, C.A.,
391 Askanas, V., Engel, W.K., Bhasin, S.*, et al.* (2001). Muscle-specific mutations accumulate with
392 aging in critical human mtDNA control sites for replication. Proc Natl Acad Sci U S A *98*,
393 4022-4027.

394 West, A.P., and Shadel, G.S. (2017). Mitochondrial DNA in innate immune responses and
395 inflammatory pathology. Nat Rev Immunol *17*, 363-375.

396 Ye, X., Sun, X., Starovoytov, V., and Cai, Q. (2015). Parkin-mediated mitophagy in mutant
397 hAPP neurons and Alzheimer's disease patient brains. Hum Mol Genet *24*, 2938-2951.
398